Astronomy
&
Astrophysics

Molecular excitation in the Eagle nebula's fingers

F. Schuller[1], S. Leurini[1], C. Hieret[1], K. M. Menten[1], S. D. Philipp[1], R. Güsten[1], P. Schilke[1], and L.-Å. Nyman[2]

[1] Max-Planck-Institut für Radioastronomie, Auf dem Hügel 69, 53121 Bonn, Germany
   e-mail: schuller@mpifr-bonn.mpg.de
[2] European Southern Observatory, Alonso de Cordova 3107, Casilla 19001, Santiago 19, Chile

ABSTRACT

Context. The M 16 nebula is a relatively nearby HII region, powered by O stars from the open cluster NGC 6611, which borders to a Giant Molecular Cloud. Radiation from these hot stars has sculpted columns of dense obscuring material on a few arcmin scales. The interface between these pillars and the hot ionised medium provides a textbook example of a Photodissociation Region (PDR).
Aims. To constrain the physical conditions of the atomic and molecular material with submillimeter spectroscopic observations.
Methods. We used the APEX submillimeter telescope to map a $\sim 3' \times 3'$ region in the CO $J = 3–2$, 4–3 and 7–6 rotational lines, and a subregion in atomic carbon lines. We also observed $C^{18}O(3–2)$ and CO(7–6) with longer integrations on five peaks found in the CO(3–2) map. The large scale structure of the pillars is derived from the molecular lines' emission distribution. We estimate the magnitude of the velocity gradient at the tips of the pillars and use LVG modelling to constrain their densities and temperatures. Excitation temperatures and carbon column densities are derived from the atomic carbon lines.
Results. The atomic carbon lines are optically thin and excitation temperatures are of order 60 K to 100 K, well consistent with observations of other HII region-molecular cloud interfaces. We derive somewhat lower temperatures from the CO line ratios, of order 40 K. The CI/CO ratio is around 0.1 at the fingers tips.

Key words. HII regions – ISM: individual objects: M 16 – radio lines: ISM – submillimeter

1. Introduction

The interplay of massive stars with their surrounding interstellar medium, though of critical importance in the energy budget of a galaxy, is still poorly understood due to observational limitations, and to the generally large distance to high mass star forming regions. Located only 1.8 ± 0.5 kpc away (Bonatto et al. 2006), the M 16 (Eagle) nebula is one of the best templates for detailed analysis of the environment of high-mass stars. This nebula is associated with the NGC 6611 star cluster, which contains more than two dozen stars of spectral type earlier than B0 (Duchêne et al. 2001) and hundreds of lower mass stars and has an age of 1.3 ± 0.3 Myr (Bonatto et al. 2006). To the south of this cluster, the radiation from these hot stars has sculpted columns of dense obscuring material on a few arcmin scales, usually referred to as "fingers" or "pillars", of which Hester et al. (1996) presented stunning Hubble Space Telescope (HST) images. The boundary between the HII region and the dense molecular gas provides an archetype of a Photodissociation Region (PDR).

Indications of present-day star formation near the tips of the fingers are seen e.g. at infrared (IR) wavelengths (Thompson et al. 2002). The fingers have been mapped in the $J = 1–0$ line of CO and isotopologues by Pound (1998) with the BIMA array. White et al. (1999) used the JCMT 15 m and OSO 20 m radiotelescopes to map the same region in various molecular lines and in the submm continuum. They report CO(2–1) and CO(3–2) peak brightness temperatures above 40 K and 60 K, respectively, and a factor 2–3 lower temperature in CO(1–0).

Here we report on new observations in two submillimeter windows, conducted with the APEX[1] 12 m telescope. We have mapped an area covering the three pillars in CO rotational lines. In addition, we have mapped the fingertips in the $^3P_1–^3P_0$ and $^3P_2–^3P_1$ transitions of atomic carbon to probe the PDR. Details on the observations are given in Sect. 2. Results of modelling the dense molecular phase are addressed in Sect. 3, while the properties of the PDR itself are discussed in Sect. 4.

2. Observations

We have used the dual colour FLASH heterodyne receiver (Heyminck et al., this volume) to simultaneously observe the $J = 4–3$ and $J = 7–6$ lines of CO, as well as, also simultaneously, the 492 GHz and 809 GHz transitions of atomic carbon. The CO $J = 3–2$ line was mapped using the APEX-2a (Risacher et al., this volume) facility receiver. With both instruments, the backend used was the MPIfR Fast Fourier Transform Spectrometer (Klein et al., this volume), which provides 16 384 spectral channels over a 1 GHz bandwidth. Calibration was done by observing the sky, hot and cold loads and using an atmospheric model. This provides spectra in antenna temperature unit. Efficiencies have been determined on observations of planets for all receivers (Güsten et al., this volume) and applied to the measured signal. The spectra were then converted to the main beam temperature scale, using beam efficiencies of 0.73 at 345 GHz, 0.60 at 460 and 492 GHz, and 0.47 at 809 GHz. The overall calibration uncertainty of the data is estimated to be $\sim 20\%$. The pointing was checked every hour on the nearby sources Sgr B2(N) and G10.62–0.38 and was found to be stable within $3''$. However,

Table 1. Log of the observations. The T_{sys} column gives typical single side band system temperatures.

Transition	Frequency [GHz]	T_{sys} [K]	Date of observation
CO(3–2)	345.796	230	17–18 Nov. 2005
C^{18}O(3–2)	329.331	330	18 Nov. 2005
CO(4–3)	461.041	800	28 Jul. 2005 +
			1 Oct. 2005 +
CO(7–6)	806.652	2500	7–8 Apr. 2006
CI $^3P_1$–$^3P_0$	492.161	850	02 Aug. 2005 +
CI $^3P_2$–$^3P_1$	809.342	2000	04–05 Oct. 2005

parts of the observations were done at elevations above 80°, where the tracking becomes somewhat less accurate.

We performed position switched observations, with a fixed reference position to the east of the easternmost finger and at an offset of $120''$, $0''$ relative to our $(0, 0)$ position, which is $\alpha_{2000} = 18^h18^m52\overset{s}{.}19$, $\delta_{2000} = -13°48'58\overset{''}{.}6$. All offsets used in the following are relative to that position. We mapped a $2' \times 2'$ area with $7''$ spacing in both directions in CO(4–3) and CO(7–6), and $3' \times 3'$ with $10''$ spacing in CO(3–2). Based on the peaks found in the CO(3–2) map, five positions were also observed in the (3–2) transition of C^{18}O (see Sect. 3.3 and Table 2). Due to moderate weather conditions for CO(7–6) in the first observing runs, we repeated the CO(4–3) and (7–6) observations with longer integrations in April 2006 toward these peak positions. A limited $40'' \times 20''$ region covering the tip of the eastern most finger and a $30''$ strip on the tip of the middle finger were mapped in atomic carbon lines, with $7''$ spacing in both cases (Sect. 4). The log of the observations is reported in Table 1.

3. Molecular material

3.1. Large scale structure

A map of the CO(3–2) emission is shown superimposed on an 8 μm Spitzer image in Fig. 1. The 8 μm emission mostly comes from small dust grains and polycyclic aromatic hydrocarbons (PAHs) excited by the incoming radiation. It traces the edge of the dusty structure, while the molecular emission peaks somewhat deeper in the columns, as expected from a transition from ionised to atomic to molecular medium. The integrated intensity in the CO(4–3) line is shown overlaid on the HST data from Hester et al. (1996) in Fig. 2. Given the pointing uncertainties mentioned above, the structure of the CO(4–3) agrees remarkably well with the columns of dust seen in the HST image.

The 3-dimensional kinematics of the region has been discussed e.g. by Pound (1998). Our data are fully consistent with the picture that they derived. In particular, our data confirm that the CO emission along the easternmost column arises from two distinct cores. We also observed velocity gradients (see below) with position angles mostly pointing to the nearby O stars.

3.2. Dense cores

On the tip of the eastern most column, we measure a difference in V_{LSR} of 2.15 ± 0.07 km s^{-1} between offset positions $(+10'', +20'')$ and $(0, -10'')$ in the CO(3–2) line. This corresponds to a velocity gradient of 7.8 ± 0.3 km s^{-1} pc^{-1}, in good agreement with Pound (1998), who found a value of 7.1 km s^{-1} pc^{-1} when scaled to the distance of 1.8 kpc used in the present paper.

We derived excitation temperatures by correcting the main beam temperatures for the Rayleigh-Jeans approximation,
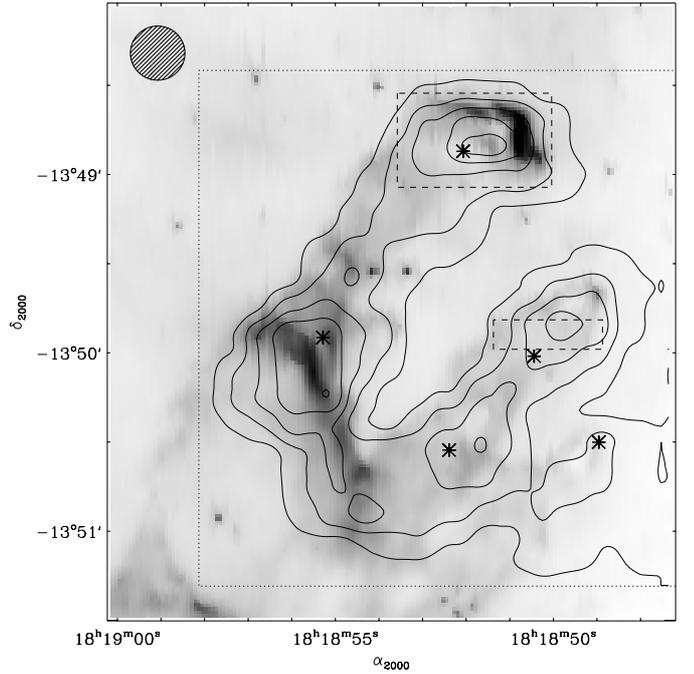
Fig. 1. Contour map of the CO(3–2) emission, integrated over the +20 to +30 km s^{-1} V_{LSR} range, overlaid on a Spitzer 8 μm image from the GLIMPSE survey (Benjamin et al. 2003). Contours correspond to 30, 60,... 180 K km s^{-1} in integrated T_{MB}. The APEX beam at 345 GHz is shown in the upper left corner. The dotted line shows the limits of our CO(3–2) data. The asterisks show the positions where we ran LVG modelling (Sect. 3.3) and the frames drawn in dashed lines delineate the areas mapped in atomic carbon lines (Sect. 4).

assuming that the CO lines are optically thick and that the emission is filling the main beam. At position offset $(-10'', 0)$, the three transitions of CO give similar temperatures around 54 ± 7 K, suggesting that the molecular material is close to thermal equilibrium.

3.3. Gas temperature and column density

To determine the physical parameters at different positions in the fingers, we used the CO observations and a spherically symmetric Large Velocity Gradient (LVG) statistical equilibrium code, with the cosmic background as only radiation field. In order to compare the CO(7–6) and CO(4–3) observations with the LVG results, we smoothed the CO(7–6) data to the spatial resolution of the CO(4–3).

From the CO(3–2)/C^{18}O(3–2) line ratios, we estimated the optical depths of the CO(3–2) lines, and derived CO column densities by comparing with LVG simulations. In this calculation, we used ^{16}O/^{18}O = 407, as derived from the relation given by Wilson & Rood (1994) as a function of galactocentric distance, with $d_{GC} = 6.3$ kpc (Bonatto et al. 2006). For positon $(-10'', 0'')$, the non-detection of C^{18}O(3–2) at $v_{LSR} = 23.6$ km s^{-1} gives an upper limit to the CO column density of 10^{17} cm^{-2}. For the other positions, the LVG modelling gives a range of possible column densities, as reported in Table 2; our results agree with the average CO column density derived by Pound (1998) and with the C^{18}O column densities of White et al. (1999).

Using these values for the CO column densities, we further constrained the gas properties by running LVG calculations for several densities and temperatures. We found that the CO(7–6) and (4–3) lines are thermalized for densities higher than a few
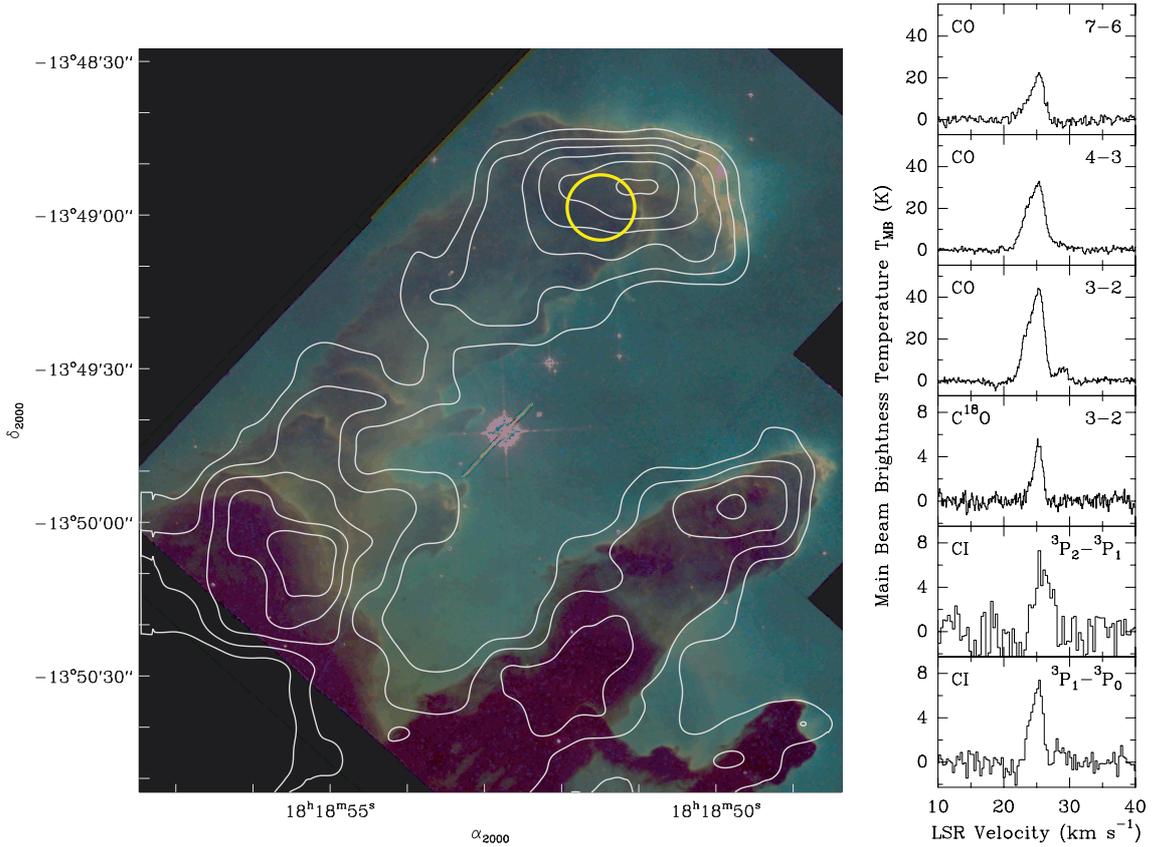
Fig. 2. *Left hand side*: contour map of the CO(4–3) emission, integrated over 20–28 km s^{-1}, overlaid on an HST composite image ([OIII], H$_\alpha$ and [SII] filters) from Hester et al. (1996). Contour levels are shown for $\int T_{MB} dv$ from 40 to 165 K km s^{-1} in steps of 25 K km s^{-1}. The circle marks the size of the APEX beam for the CO (4–3) line and is placed at the position toward which the spectra in the right hand side of this figure were taken. *Right hand side, top to bottom*: spectra of the CO (7–6), (4–3), (3–2), the C^{18}O (3–2) and the CI ^{3}P$_2$–^{3}P$_1$ and ^{3}P$_1$–^{3}P$_0$ lines taken toward the $-10''$, 0 offset position marked in the left part of this figure.

Table 2. Results of the CO lines modelling. Columns 4 and 5 give the gas kinetic temperatures, as derived by comparing the observed T_{MB} of CO(4–3) and (7–6), respectively, with the LVG models. Offsets are relative to the (0, 0) position given in Sect. 2.

Offset [$''$, $''$]	v_{lsr} [km s^{-1}]	N(CO) [cm^{-2}]	$T_{CO(4-3)}$ [K]	$T_{CO(7-6)}$ [K]
$-10, 0$	23.6	$\leq 1 \times 10^{17}$	45 ± 7	
$-10, 0$	25.4	$8 \times 10^{17} - 1 \times 10^{19}$	54 ± 8	56 ± 9
$+40, -60$	24.6	$8 \times 10^{17} - 6 \times 10^{18}$	40 ± 6	42 ± 6
$-30, -70$	22.4	$6 \times 10^{17} - 1 \times 10^{19}$	50 ± 9	57 ± 7
$-50, -100$	21.3	$6 \times 10^{17} - 1 \times 10^{19}$	30 ± 4	32 ± 6
$0, -100$	21.4	$2 \times 10^{17} - 6 \times 10^{18}$	51 ± 9	47 ± 7

10^4 cm^{-3}. Both lines are optically thick at the column densities that we computed (Table 2); therefore, the observed T_{MB} give direct measures of the kinetic temperature of the gas. Other authors (Pound 1998; White et al. 1999) reported densities of $3–5 \times 10^4$ cm^{-3} in the fingers, with higher values ($\sim 2 \times 10^5$ cm^{-3}) at the fingertips. Thus, the temperatures reported in Table 2 are derived from LVG models with densities above 10^4 cm^{-3}. For lower densities, they would correspond to lower limits to the true kinetic temperature of the gas. Our estimates are computed by assuming beam filling factors of 1. The temperatures we derived do not change significantly over the range of column densities computed for each position and the variation is, in any case, within the error bars, corresponding to a calibration uncertainty of 20% for each line.
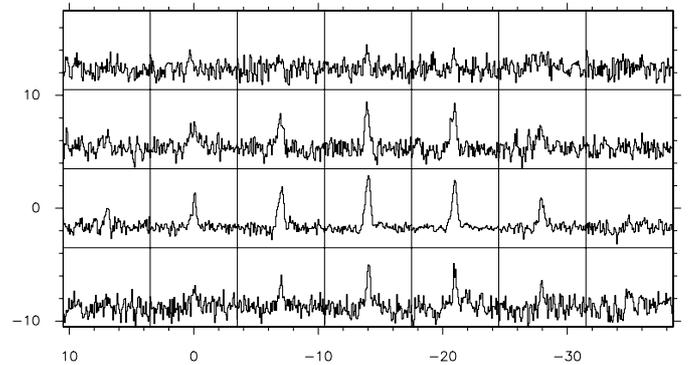
Fig. 3. Map of the atomic carbon line at 492 GHz covering the edge of the northernmost finger. Axes show the offsets (in arcsec) with respect to the (0, 0) position (Sect. 2). Each spectrum is shown over the 10–40 km s^{-1} range in V_{LSR}, with a vertical scale going from –5 to +15 K in T_{MB}. Excitation temperatures derived from the 492 GHz and 809 GHz transitions are given in Table 3.

4. Atomic carbon lines

In the north-south direction, [CI] 492 GHz extends over at least $\sim 30''$, or 0.25 pc at the distance of M 16 (see map in Fig. 3). Using Eqs. (7) and (8) in Zmuidzinas et al. (1988), we derived excitation temperatures and opacities for both [CI] lines, using the measured main beam temperatures for both transitions. This assumes a uniform excitation temperature, and that the levels are

Table 3. Peak main beam temperatures of the [CI] lines. The excitation temperatures and line opacities are computed after Zmuidzinas et al. (1988), using the T_{MB} scale for both lines. Typical uncertainties are of order –20 K to +30 K for T_{ex}, and ±0.1 for opacities (see text). Column densities are derived from T_{ex} and $\tau(1-0)$ after Keene et al. (1985). Offsets are relative to the (0, 0) position (Sect. 2).

Offset		$T_{MB}(1-0)$	v_{LSR}	$T_{MB}(2-1)$	v_{LSR}	T_{ex}	$\tau(1-0)$	$\tau(2-1)$	$N(CI)$
['']	['']	[K]	[km s^{-1}]	[K]	[km s^{-1}]	[K]			[cm^{-2}]
–21	0	10.8	25.37 (0.02)	11.6	25.94 (0.06)	61	0.24	0.31	3.2×10^{17}
–14	0	12.2	25.54 (0.03)	14.3	25.76 (0.09)	71	0.23	0.31	3.8×10^{17}
–7	0	9.2	25.60 (0.06)	10.4	25.70 (0.17)	66	0.18	0.24	2.9×10^{17}
0	0	7.2	25.75 (0.06)	9.7	25.52 (0.10)	93	0.09	0.14	1.8×10^{17}
–35	–63	10.3	23.10 (0.06)	14.3	22.95 (0.12)	103	0.12	0.19	2.6×10^{17}

thermally populated. Since both lines were observed simultaneously, systematic errors should cancel out in this analysis, so that using a 10% uncertainty for each measured T_{MB} is reasonable. The resulting uncertainties are of order –20 to +30 K for T_{ex} and ±0.1 for opacities.

The results are shown in Table 3 for the central part of the map covering the tip of the first finger, and for offset position (–35'', 63'') at the tip of the second finger, where we have good S/N spectra in both transitions. We find optically thin lines, with opacities in the range 0.1–0.3, and excitation temperatures in the range 60–100 K, i.e. in the upper part of the temperature range computed by Zmuidzinas et al. (1988) in various sources. We also derived excitation temperatures from LVG modelling, and found similar results, in the range 80–120 K.

We computed CI column densities using the same formalism as described in the Appendix of Keene et al. (1985). They are reported in the last column of Table 3. The corresponding CI/CO ratios are around 0.1 at the tips of both fingers. However, CI and C^{18}O emissions are likely to trace distinct material, and additional observations are considered to constrain the variations of CI/CO in the region.

5. Summary and conclusion

We have observed the transitions of atomic carbon for the first time toward the M 16 nebula, and derived excitation temperatures for the atomic material around 60–100 K, similar to the values found in other HII region-molecular cloud interfaces. The kinetic temperatures derived from CO transitions seem somewhat lower, around 40 K in most positions. This is consistent with the picture where the atomic carbon traces the PDR at the edge of the dense molecular columns. The CI to CO ratio is ~0.1 at the fingers tips. Additional observations and comparison with PDR models are needed to further constrain the atomic to molecular transition.

References

Benjamin, R. A., Churchwell, E. B., Babler, B., et al. 2003, PASP, 115, 953
Bonatto, C., Santos, J. F. C., & Bica, E. 2006, A&A, 445, 567
Duchêne, G., Simon, T., Eislöffel, J., & Bouvier, J. 2001, A&A, 379, 147
Hester, J., Scowen, P. A., Sankrit, R., et al. 1996, AJ, 111, 2349
Keene, J., Blake, G. A., Phillips, T. G., Huggins, P. J., & Beichman, C. A. 1985, ApJ, 299, 967
Pound, M. W. 1998, ApJ, 493, L113
Thompson, R. I., Smith, B. A., & Hester, J. J. 2002, ApJ, 570, 749
White, G. J., Nelson, R. P., Holland, W. S., et al. 1999, A&A, 342, 233
Wilson, T. L., & Rood, R. 1994, ARA&A, 32, 191
Zmuidzinas, J., Betz, A. L., Boreiko, R. T., & Goldhaber, D. M. 1988, ApJ, 335, 774